

Quantum Control of Atom-Ion Charge Exchange via Light-induced Conical Intersections

Hui Li,^{1,*} Ming Li,¹ Alexander Petrov,¹ Eite Tiesinga,² and Svetlana Kotochigova^{1,†}

¹*Department of Physics, Temple University, Philadelphia, Pennsylvania 19122, USA*

²*Joint Quantum Institute, National Institute of Standards and Technology
and University of Maryland, Gaithersburg, Maryland 20899, USA*

(Dated: April 18, 2023)

Conical intersections are crossing points or lines between two or more adiabatic electronic potential energy surfaces in the multi-dimensional coordinate space of colliding atoms and molecules. Conical intersections and corresponding non-adiabatic coupling can greatly affect molecular dynamics and chemical properties. In this paper, we predict significant or measurable non-adiabatic effects in an ultracold atom-ion charge-exchange reaction in the presence of laser-induced conical intersections (LICIs). We investigate the fundamental physics of these LICIs on molecular reactivity under unique conditions: those of relatively low laser intensity of 10^8 W/cm^2 and ultracold temperatures below 1 mK. We predict irregular interference effects in the charge-exchange rate coefficients between K and Ca^+ as functions of laser frequency. These irregularities occur in our system due to the presence of two LICIs. To further elucidate the role of the LICIs on the reaction dynamics, we compare these rate coefficients with those computed for a system where the CIs have been “removed”. In the laser frequency window, where conical interactions are present, the difference in rate coefficients can be as large as $10^{-9} \text{ cm}^3/\text{s}$.

I. INTRODUCTION

Theoretical descriptions of many chemical processes are often based on the Born-Oppenheimer (BO) approximation [1]. This approximation relies on the observation that the motion of electrons and atomic nuclei occurs on different time or energy scales and thus allows the separation of electronic and nuclear degrees of freedom. The resulting model simplification minimizes computational efforts.

There exist, however, many cases where the coupling between electronic and nuclear motion is non-negligible and the BO approximation breaks down [2]. In particular, the potential energy surfaces of electronic states with the same symmetry of polyatomic molecules with three or more atoms can be degenerate at crossing points or curves in the multi-dimensional space of the nuclear coordinates. These crossings are called conical intersections (CIs). Generally, CIs form a seam of $3N - 8$ dimensions, where N is the number of atoms in the molecule. At these crossings strong non-adiabatic transitions between electronic states occur.

Conical intersections between molecular electronic potential surfaces thus greatly affect molecular dynamics and chemical reactivity. Conditions under which conical intersections occur have been extensively reviewed Refs. [3–5]. Naturally occurring CIs play a crucial role in photochemistry and photobiology as well as optical and superconductor physics [3, 6–8]. Clearly, the location of such CIs and the strength of the related non-

adiabatic couplings are inherent properties of the atoms in the molecule and are difficult to manipulate or control.

When molecules are exposed to resonant laser light, however, new features can emerge. Moiseyev *et al.*[9] showed that with laser light it is possible to create a conceptually different kind of CI even in diatomic molecules, a so-called light-induced conical intersection (LICI). In contrast to natural conical intersections the characteristics of LICIs are easily modified by the parameters of the laser field. The internuclear positions of LICIs are determined by the laser frequency and the direction of the laser polarization ϵ . That is, the angle θ between a molecular axis and the direction of polarization adds a motional degree of freedom and a controllable CI can appear.

Initial theoretical descriptions of LICIs [9–13] focused on the diatomic Na_2 molecule interacting with either a retroreflected laser beam creating a spatial standing wave potential for the dimer or with short but strong laser pulses. For both implementations this leads to a degeneracy of “dressed” electronic states in a two-dimensional space, where one of the coordinates is the separation R between the sodium atoms. Study of the core excited CO^* molecule in x-ray regimes [14, 15] show that LICIs should lead to nonadiabatic transitions between electronic, vibrational, and rotational degrees of freedom of the diatomic molecule. In addition, with the readily availability of laser-cooled atoms there is also a growing interest in these concepts applied to ultracold atom-atom collision [16–18]. The dramatic effect of the light-induced conical intersection on the photodissociation and photofragmentation of the D_2^+ molecule was demonstrated in [19–21]. Recently, Csehi *et al.*[22, 23] in a theoretical studies showed that LICI in diatomics can be created even by quantized radiation field in an optical cavity.

* Present address: JILA, University of Colorado, Boulder, Colorado 80309, USA

† skotoch@temple.edu

Light-induced conical intersections have been studied experimentally with ultrafast molecular processes. Kim *et al.*[24] found that a LICI can control the isomerization of 1,3-cyclohexadiene, while Corrales *et al.*[25] investigated the transition from a weak- to strong-fields in the LICI-induced dissociation of polyatomic methyl iodide. Quantum interference in the dissociation of H_2^+ initiated by a LICI was observed by Natan *et al.*[26] with focussed 30 fs laser pulses with a peak intensity of $2 \times 10^{13} \text{ W/cm}^2$. Finally, Kübel *et al.*[27] performed detailed investigations of the light-induced molecular potentials in the same molecular system. They demonstrated the presence of distortions in the nonadiabatic potential energy surfaces from modulations in the angular distribution of the reaction paths.

In this paper, we investigate the role played by LICIs in the charge-exchange reaction between ground-state ${}^{40}\text{Ca}^+$ ions and neutral ground-state ${}^{39}\text{K}$ atoms prepared in well-controlled quantum states and at ultracold collision energies. We envision two experimental realizations of our ideas. The first corresponds to one where ultracold K and Ca^+ are stored in overlapping optical dipole and Paul traps, respectively, and the frequency of a linearly polarized laser is tuned. In a dressed-state picture or with Floquet analysis, dressed molecular states satisfy the conditions required for LICIs as schematically shown in Fig. 1. Two dressed adiabatic molecular states as functions of the atom-atom separation R and the angle between the inter-atomic axis and the laser polarization θ touch forming one or two LICIs at one or two pairs (R, θ) . The non-trivial dependence of the charge-exchange rate coefficient on laser frequency can then reveal the presence of LICIs. Our simulations will be restricted to this realization.

A second realization, not studied here, to show the presence of LICIs might correspond to the case where spatially separate clouds of ultracold K and Ca^+ are accelerated towards each other to form a KCa^+ quasimolecule with an oriented interatomic axis. In the presence of a linearly polarized laser, the behavior of the charge-exchange reaction rate as a function of the angle between the collision axis and the laser polarization direction can then reveal the presence of LICIs. Prototype experiments studying oriented collisions between two ultracold neutral atom clouds can be found in Ref. [28].

Our model of the former realization allows us to investigate the effect of the multiple “pathways” around the two LICIs that occur in our system. These pathways lead to interference patterns in the charge-exchange rate coefficient as function of the laser frequency and intensity. Moreover, shape resonances in the rate coefficients are observed as function of the atom-ion collision energy. In a theoretical model, we can “switch” on and off the CI to further elucidate effect of a CI on the reaction dynamics.

It is important to note that there are many examples in the literature devoted to increasing atom-ion charge-exchange reaction rates with external radiation [29–40]. In most of these examples, the research focused on col-

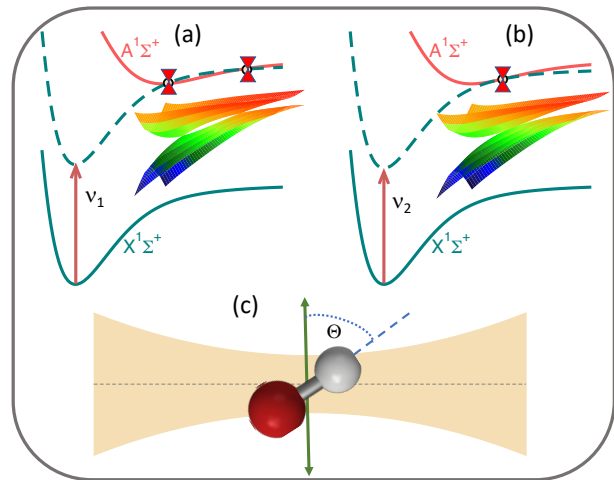


FIG. 1. Schematic of the LICI-enhanced charge-exchange reaction in ultracold $\text{K}+\text{Ca}^+$ collisions. Panels a) and b) show the photon dressing of the radial diabatic potentials (line drawings) and two-dimensional adiabatic potentials of KCa^+ as functions of radial separation R and orientation θ (colored three-dimensional surfaces) with (a) two conical intersections and (b) with one glancing intersection in the R - θ plane, respectively. The laser photon frequencies ν_i in panels a) and b) are $\nu_1/c = 13\,966 \text{ cm}^{-1}$ and $\nu_2/c = 13\,889 \text{ cm}^{-1}$, respectively. Here, c is the speed of light in vacuum. Panel c) shows the definition of θ , the angle between the inter-atomic axis (blue dashed line) connecting the atom and the ion (red and grey balls) and the direction of the linear laser polarization (green double arrow). The orange region represents the laser intensity profile (not to scale).

liding neutral and ionic atoms where one or both of the colliding partners are prepared in optically excited electronic states, which led to a rich variety of exit channels. In these studies, the topology of a LICI was not invoked to explain the data or LICIs were not even present. For example, in a recent paper in collaboration with K. Brown’s group [40], we demonstrated that colliding neutral ${}^{39}\text{K}$ atoms and optically excited ${}^{40}\text{Ca}^+$ ions confined in spatially overlapping magneto-optical and Paul traps, respectively, exhibit large charge-exchange rates. In this case LICIs were not present. The measured charge-exchange rate coefficients were in good agreement with our theoretical estimates.

II. THEORETICAL MODEL

Ultracold collisions of K and Ca^+ , both in their doublet ${}^2\text{S}$ electronic ground state, form molecular states that are superpositions of the excited singlet $\text{A}^1\Sigma^+$ and energetically lowest triplet $\text{a}^3\Sigma^+$ states [40], where only the $\text{A}^1\Sigma^+$ component leads to radiative decay into bound states of the singlet ground $\text{X}^1\Sigma^+$ K^+Ca potential or the $\text{K}^+({}^1\text{S})$ and $\text{Ca}({}^1\text{S})$ continuum. This decay into the continuum corresponds to charge exchange with a small

charge-exchange rate coefficient on the order of 10^{-14} cm³/s [40].

In the presence of laser light, the charge-exchange rate coefficient can be enhanced. Figure 1 schematically shows our theoretical model of the dressed K and Ca⁺ collision. The X¹Σ⁺ and A¹Σ⁺ states are dressed with photons of energy $h\nu$ of the laser allowing for additional charge-exchange processes. Here, ν is the photon frequency and h is the Planck constant. In Fig. 1(a) the potential of the A¹Σ⁺ state dressed with one photon crosses the potential of the X¹Σ⁺ state twice when the photon wavelength is 716 nm. For a photon wavelength of 720 nm in Fig. 1(b), we create a glancing or Renner-Teller intersection [41] of A¹Σ⁺ and X¹Σ⁺ state potentials with a quadratic dependence on the nuclear coordinates. The colored surface plots in these panels show that the two intersections and the one glancing intersection, respectively, are conical intersections in the R - θ plane for the dressed adiabatic potentials that include the atom-light coupling. In this article, the continuous-wave laser light is linearly polarized along the space-fixed z axis and Fig. 1(c) shows the angle θ between the inter-atomic axis and the polarization of the laser light.

The dressed-state Hamiltonian for our system is

$$H = -\frac{\hbar^2}{2\mu_r} \frac{d^2}{dR^2} + \frac{\mathbf{L}^2}{2\mu_r R^2} + V^{\text{mol}}(R) + V^{\text{rad}}(\mathbf{R}) + H_{\text{laser}}, \quad (1)$$

where R is the internuclear separation, μ_r is the reduced mass, \mathbf{L} is the molecular orbital angular momentum operator with eigenstates $|\ell m_\ell\rangle$ and projection quantum number m_ℓ defined with respect to our space-fixed z axis, $V^{\text{mol}}(R)$ is the electronic Hamiltonian

$$V^{\text{mol}}(R) = \begin{pmatrix} V_1(R) & 0 \\ 0 & V_2(R) \end{pmatrix}, \quad (2)$$

where $V_1(R)$ and $V_2(R)$ are the isotropic potential energies of the singlet X¹Σ⁺ and A¹Σ⁺ electronic states, respectively. Their electronic wavefunctions will be denoted by $|1\rangle$ and $|2\rangle$. We use the potentials regarding their computations and data tables are given in Supplemental Material. Note that for $R \rightarrow \infty$, we have $V_2(R) - V_1(R) \rightarrow \Delta \equiv +hc \times 14296.114$ cm⁻¹ derived from neutral K and neutral Ca ionization energies found in Ref. [42]. The dissociation energy or depth and equilibrium separation of the A¹Σ⁺ state potential are $D_e = hc \times 1090$ cm⁻¹ and $R_e = 12.9a_0$. Here, a_0 is the Bohr radius. The depth of the X¹Σ⁺ potential is just over four times larger than that of the A¹Σ⁺ state.

The fourth term in Eq. (1), $V^{\text{rad}}(\mathbf{R})$, describes the electric dipole interaction with the laser field. In a body-fixed coordinate system, it is proportional to $\cos \theta$, where $\theta \in [0, \pi]$ is the angle between the internuclear axis and the polarization of the laser field. Hence, the molecule-field interaction is anisotropic. In the rotating wave approximation,

$$V^{\text{rad}}(\mathbf{R}) = -d(R) \sqrt{2\pi h\nu/V} \cos \theta [a^\dagger |1\rangle \langle 2| + h.c.], \quad (3)$$

where $d(R)$ is the R -dependent molecular electronic transition dipole moment between the X¹Σ⁺ and A¹Σ⁺ states and abbreviation *h.c.* stands for the hermite conjugate. Finally, $H_{\text{laser}} = h\nu a^\dagger a$ describes the energy in our laser field with photon creation and annihilation operators a and a^\dagger in volume V , respectively. Its eigenstates are $|n\rangle$ with energy $n\nu$ for non-negative integers or photon numbers n . The operator $V^{\text{rad}}(\mathbf{R})$ has non-zero matrix elements between states that differ by one photon number. Effects of the permanent dipole moments of the X¹Σ⁺ and A¹Σ⁺ states are neglected. They do not lead to charge exchange. We use the transition dipole moment from Ref. [40]. See Supplemental Material for a description and a data table. Potential energy curves, spectroscopic constants, and transition electric dipole moments of K⁺Ca were also determined and analyzed in Ref. [43].

For coupled-channels calculations, we use the basis $|i; \ell m_\ell; n\rangle \equiv |i\rangle |\ell m_\ell\rangle |n\rangle$ with $i = 1, 2$. In this basis \mathbf{L}^2 , V^{mol} , and H_{laser} are diagonal. Only, $V^{\text{rad}}(\mathbf{R})$ couples basis functions with matrix elements

$$\begin{aligned} & \langle 1; \ell m_\ell; n + 1 | V^{\text{rad}}(\mathbf{R}) | 2; \ell' m'_\ell; n \rangle \\ &= -d(R) \sqrt{\frac{2\pi I}{c}} \sqrt{\frac{2\ell' + 1}{2\ell + 1}} C_{10, \ell' m'_\ell}^{\ell m_\ell} C_{10, \ell' 0}^{\ell 0}, \end{aligned} \quad (4)$$

where I is the laser intensity and $C_{j_1 m_1, j_2 m_2}^{j m}$ are Clebsch-Gordan coefficients. For our laser polarization $m'_\ell = m_\ell$ and the matrix element is only non-zero when $\ell + \ell'$ is odd. The dressed state picture, pioneered by C. Cohen-Tannoudji *et al.* [44] and as used here, is for large photon number $n \gg 1$ equivalent to Floquet theory based on a classical time-dependent description of light. For $n \gg 1$, it is appropriate to replace the photon number dependence of the matrix element in Eq. (4) by the mean photon number (per unit area) in the laser and thus by laser intensity I as it is proportional to the mean photon number. As we will show the change in photon number due to the molecular processes is small even at our largest laser intensities.

The charge-exchange rate coefficient from $|1\rangle$ with n photons and ultracold collision energy E is given by

$$K = \frac{\hbar\pi}{\mu_r k} \sum_{\ell, \ell'=0}^{\ell_{\text{max}}} \sum_{m_\ell} \sum_{n'=n-\delta n}^{n+\delta n} |T_{2, \ell' m_\ell, n' \leftarrow 1, \ell, m_\ell, n}|^2, \quad (5)$$

where $k = \sqrt{2\mu_r E/\hbar^2}$ is collisional wave vector, m_ℓ runs from $-\min(\ell, \ell')$ to $\min(\ell, \ell')$, and \hbar is the reduced Planck constant. The quantities $T_{f \leftarrow i}$ are T-matrix elements obtained from scattering solutions of Eq. (1), where the photon numbers changes by no more than $\delta n=1$ or 2, and partial waves ℓ from 0 to $\ell_{\text{max}} = 6$ are coupled, sufficient for convergence at collision energies E up to $k \times 1$ mK and laser intensities up to 10^8 W/cm². Here, k is the Boltzmann constant. We find that the main contribution to K comes from T-matrix elements with $n' = n + 1$, corresponding to the transition $|1\rangle + n\nu \rightarrow |2\rangle + (n + 1)\nu$.

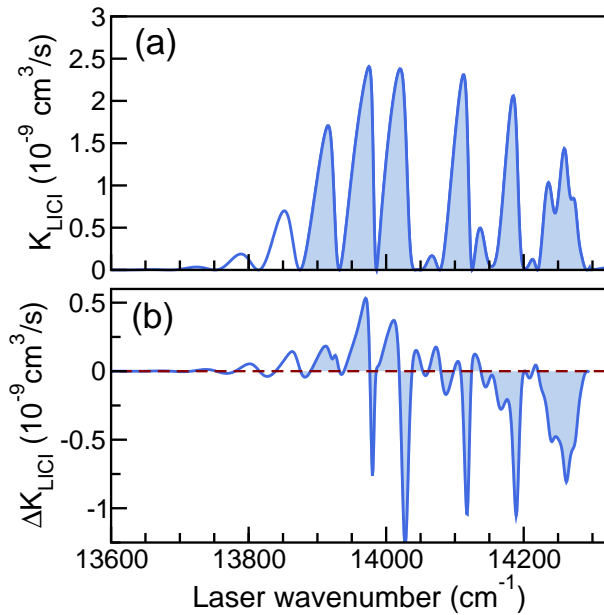


FIG. 2. a) The charge-exchange rate coefficient K_{LICI} as a function of laser wavenumber at a collision energy of $E/k = 7 \mu\text{K}$ and a laser intensity of $I = 10^8 \text{ W/cm}^2$. The shaded light-blue region indicates the frequency region where interferences between pathways around the two conical intersections occur. b) The difference $\Delta K_{\text{LICI}} = K_{\text{no-LICI}} - K_{\text{LICI}}$ as a function of laser wavenumber at $E/k = 7 \mu\text{K}$ and $I = 10^8 \text{ W/cm}^2$. Here, $K_{\text{no-LICI}}$ and K_{LICI} are charge-exchange rate coefficients computed without and with the conical intersections, respectively.

In this paper, we focus on photon energies between $hc \times 13600 \text{ cm}^{-1}$ and $\Delta = hc \times 14296.114 \text{ cm}^{-1}$, to ensure the presence of up to two LICIs between the $\text{X}^1\Sigma^+$ and $\text{A}^1\Sigma^+$ potentials, as shown Fig. 1. The LICIs are best visible in the surface graphs of Figs. 1(a) and (b) corresponding to the eigenvalues of operator $V^{\text{mol}}(R) + V^{\text{rad}}(\mathbf{R})$ as functions of R and θ . The LICIs occur at $\theta = \pi/2$ with separations R_1 and R_2 , where $R_1 \leq R_2$. For the Renner-Teller intersection $R_1 = R_2 > R_e$.

III. RESULTS AND DISCUSSIONS

Interference patterns between pathways around two LICIs. We begin by investigating the effect of LICIs on rate coefficients of the charge-exchange reaction K_{LICI} by calculating the rate coefficient around a $hc \times 800 \text{ cm}^{-1}$ range of photon energies below the difference in dissociation energy of the $\text{X}^1\Sigma^+$ and $\text{A}^1\Sigma^+$ states. A representative example is shown in Fig. 2(a) for a collision energy of $E/k = 7 \mu\text{K}$ and a laser intensity of 10^8 W/cm^2 . The laser wavenumber is increased from $\nu/c = 13600 \text{ cm}^{-1}$ to $14296.114 \text{ cm}^{-1} = \Delta/hc$, where our system goes from having no LICI to one where two LICIs exist between the $\text{A}^1\Sigma^+$ and $\tilde{\text{X}}^1\Sigma^+$ potentials. We observe regular and irregular Stueckelberg oscillations, where the rate coeffi-

cient alternates between near zero values and maxima as function of ν . Below $\nu/c = 13600 \text{ cm}^{-1}$ the light-induced charge-exchange rate coefficient is below $\sim 10^{-14} \text{ cm}^3/\text{s}$ and radiative decay studied in Ref. [40] becomes the dominant means for charge exchange. For $h\nu > \Delta$ light-induced rate coefficient K_{LICI} is negligibly small as transition $|1\rangle + nh\nu \rightarrow |2\rangle + (n+1)h\nu$ is energetically forbidden.

For photon energies between $hc \times 13600 \text{ cm}^{-1}$ and $hc \times 13896 \text{ cm}^{-1}$ we observe Stueckelberg oscillations with increasing amplitude corresponding to cases where we only have avoided crossings between $\text{A}^1\Sigma^+$ and $\tilde{\text{X}}^1\Sigma^+$ potentials. The amplitude of the oscillations increases because the avoided crossing between the potentials become narrower. Starting from laser energies $hc \times 13896 \text{ cm}^{-1}$, shaded in Fig. 2(a), two conical intersections are present and the oscillation pattern of K_{LICI} is significantly distorted or irregular due to interferences between multiple pathways around the two conical intersections.

To support our claim that the irregular Stueckelberg oscillations are due to LICIs, we first analyze the charge-exchange rate coefficient for selected laser frequencies in this frequency window. Specifically, we analyze perturbative transition matrix elements between scattering wavefunctions in channels $|1; \ell m_\ell; n\rangle$ and $|2; \ell' m'_\ell; n+1\rangle$ as function of laser frequency and locate the origin of the complex constructive and destructive interferences corresponding to large and small charge-exchange rate coefficients. We define the *partial* matrix element or integral

$$M(R) = \int_0^R dr \psi_X(r) d(r) \phi_A(r), \quad (6)$$

where real-valued $\phi_A(r)$ is the single-channel $\ell = 0$ radial scattering wave function for the $\text{A}^1\Sigma^+$ potential at initial collision energy E_{initial} and real-valued $\psi_X(r)$ is the single-channel $\ell = 1$ radial scattering wave function for the $\tilde{\text{X}}^1\Sigma^+$ potential at final collision energy $E_{\text{final}} = \Delta - h\nu + E_{\text{initial}}$. For weak laser intensities, the charge-exchange rate coefficient K_{LICI} is proportional to the square of $M(R)$ for $R \rightarrow \infty$. Constructive or destructive interference implies large or small $|M(R \rightarrow \infty)|$, respectively.

We begin the analysis by showing rate coefficient K_{LICI} at collision energy of $E/k = 1 \mu\text{K}$ in Fig. 3 on a logarithmic scale. The interference pattern is similar to that observed in Fig. 2 at a larger collision energy. Figure 4 then shows the partial matrix element $M(R)$ and the integrand $\psi_X(R) d(R) \phi_A(R)$ as functions of R for an initial collision energy of $E_{\text{initial}} = 1 \mu\text{K}$ when the wavenumbers of the dressing laser are $\nu/c = 14196 \text{ cm}^{-1}$, 14056 cm^{-1} , and 13996 cm^{-1} , respectively. The product $d(R) \phi_A(R)$ is the same for the three cases and only $\psi_X(R)$ changes.

For the largest photon energy, shown in panel (a), the system has two well-separated conical intersections located at separations R_1 and R_2 with $R_1 < R_2$. They are labelled LICI-1 and LICI-2 in the figure. We also observe that the integrand is a rapidly oscillating function with R and that it approaches zero for large R as $d(R) \rightarrow 0$

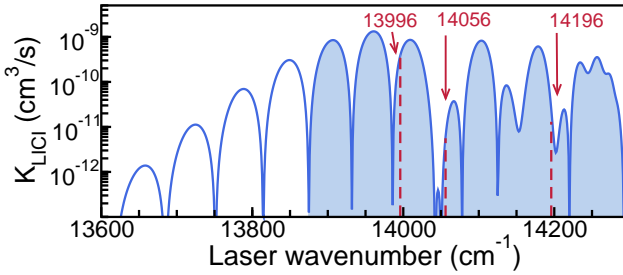


FIG. 3. The charge-exchange rate coefficient K_{LICI} as a function of laser wavenumber at $E/k = 1 \mu\text{K}$ and $I = 10^8 \text{ W/cm}^2$. The shaded light-blue region again indicates the frequency region where interferences between pathways around the two conical intersections occur. Wavenumbers 13996 cm^{-1} , 14056 cm^{-1} , and 14196 cm^{-1} with dashed red lines mark dressing conditions leading to either constructive or near destructive interference.

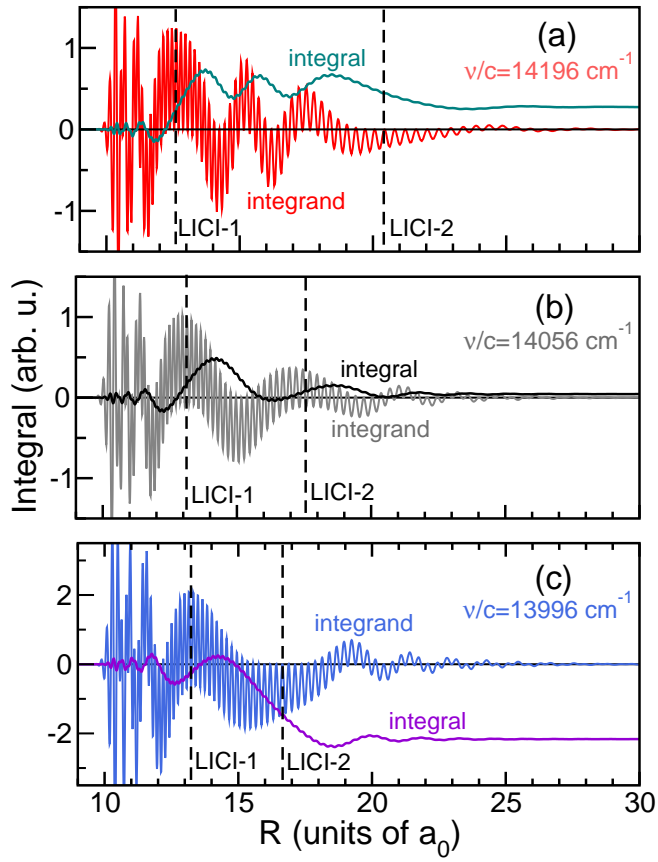


FIG. 4. Explanation of the irregular Stückelberg oscillations in the $\text{K}+\text{Ca}^+$ charge-exchange rate coefficient at a collision energy of $k \times 1 \mu\text{K}$ shown in Fig. 3 when the dressed-state potentials have two LICIs. Panels (a), (b), and (c) show the integrand and vibrationally averaged electronic transition dipole moments as functions of atom-atom separation R for laser wavenumbers $\nu/c = 14196 \text{ cm}^{-1}$, 14056 cm^{-1} , and 13996 cm^{-1} , respectively. The vertical black dashed lines labeled LICI-1 and LICI-2 in each panel correspond to the KCa^+ separations of the LICIs. The scale on the y axes of the panels are different and should not be compared.

for $R \rightarrow \infty$. Hence, we expect that cancellations but also non-zero averages will occur in the calculation of $M(R)$. Near $R = R_1$ and R_2 , where the local kinetic energies for $\tilde{X}^1\Sigma^+$ and $\text{A}^1\Sigma^+$ states are close to equal, however, the oscillations in the integrand occur around a non-zero average and, indeed, for R near R_1 the integral is seen to rapidly increase. Near $R = R_2$ the integral decreases somewhat. For all other R , $M(R)$ oscillates around a stable value. Thus, we realize that for $\nu/c = 14196 \text{ cm}^{-1}$ and $R \rightarrow \infty$ the contributions to $M(R)$ from the two LICIs partially cancel.

For the data at $\nu/c = 14056 \text{ cm}^{-1}$ in Fig. 4(b) the contributions from the two LICIs nearly cancel each other. There is destructive interference between the LICIs. For the data in panel (c) and $\nu/c = 13996 \text{ cm}^{-1}$, the radial separations of the two CIs are closest of all three cases and the contributions from the two LICIs are harder to separate. Still, the contribution to $M(R)$ near LICI-1 averages to near zero, while the contribution from LICI-2 is large. From similar figures at other kinetic energies and laser frequencies, not shown, we can understand the patterns seen in Fig. 2(a) as function of laser frequency.

We have also performed a second type of analysis to confirm that the light-induced conical intersections influence the charge-exchange process. We “removed” the conical intersections by replacing the anisotropic θ dependence in Eq. (3) with an isotropic one. In fact, we made the substitution

$$\cos \theta \rightarrow \frac{1}{\sqrt{3}} \quad (7)$$

in Eq. (3). The molecule-field interaction is now isotropic and only couples channels with the same partial wave ℓ and m_ℓ quantum numbers.

Figure 2(b) shows the difference of the charge-exchange rate coefficients $K_{\text{no-LICI}}$ and K_{LICI} as a function of laser frequency at $E/k = 1 \mu\text{K}$ and $I = 10^8 \text{ W/cm}^2$. Here, $K_{\text{no-LICI}}$ and K_{LICI} correspond to rate coefficients computed without and with conical intersections, respectively. The difference in rate coefficients can be of the same order of magnitude as K_{LICI} and be as large as $\pm 10^{-9} \text{ cm}^3/\text{s}$ in the frequency window where the conical interactions are present. For ultracold atom and ion experiments, a rate coefficient of order of $10^{-9} \text{ cm}^3/\text{s}$ is large and easily detectable.

Finally, we examine charge-exchange rate coefficients between K and Ca^+ as functions of collision energy E at $\nu/c = 13960 \text{ cm}^{-1}$ and laser intensities 10^6 W/cm^2 , 10^7 W/cm^2 , and 10^8 W/cm^2 . We remain in the ultracold collision energy domain below $k \times 1 \text{ mK}$. This case corresponds to a situation where K_{LICI} is close to maximal when $E \rightarrow 0$ and the pair of interfering conical intersections are located close together. Figure 5(a) shows rate coefficients K_{LICI} where the LICIs are present. We observe that both wide and narrow resonance features are present. Further analysis has shown that these resonances are due to shape resonances behind a ℓ -wave centrifugal barrier of the long-range

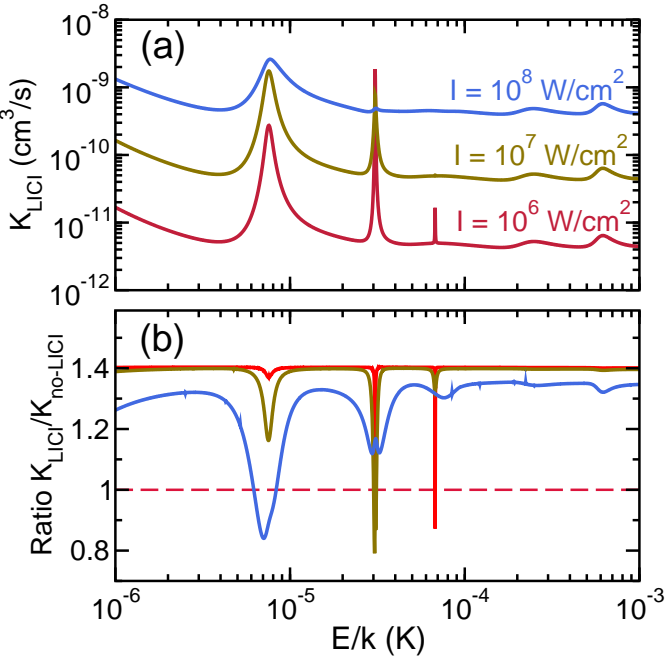


FIG. 5. The charge-exchange rate coefficient K_{LICI} computed with the CIs present (panel a) and the ratio $K_{\text{LICI}}/K_{\text{no-LICI}}$ (panel b) as functions of atom-ion collision energy at laser wavenumber $\nu/c=13960 \text{ cm}^{-1}$ and at laser intensities of $I = 10^6 \text{ W/cm}^2$ (red curve), 10^7 W/cm^2 (gold), and 10^8 W/cm^2 (blue).

$-C_4/R^4 + \hbar^2\ell(\ell+1)/(2\mu_r R^2)$ potential between a neutral atom and an ionic atom. Here, C_4 is the polarization coefficient proportional to the static polarizability of the K atom. These resonances significantly enhance the charge-exchange process. A broader resonance has an energy closer to the top of the corresponding centrifugal barrier. The rate coefficients increase approximately linearly with laser intensity, although for the largest intensity of 10^8 W/cm^2 deviations are visible. For example,

the resonances have noticeably broadened, which can be used as a signal that CIs are present.

Figure 5(b) shows the ratio $K_{\text{LICI}}/K_{\text{no-LICI}}$ of $\nu/c=13960 \text{ cm}^{-1}$ rate coefficients K_{LICI} and $K_{\text{no-LICI}}$ calculated when the LICIs are and are not present, respectively. We observe that for the smaller laser intensities the ratio is about 1.4 independent of collision energy and laser intensity, except near the shape resonances. At the higher laser intensity of 10^8 W/cm^2 the background value of the ratio of rate coefficients also changes in a measurable way, although the width and strength of the resonances are again affected more dramatically.

In Summary: We have computed charge-exchange rate coefficients of colliding K atoms and Ca^+ ions confined in hybrid atom-ion traps at ultracold temperatures in the presence of a near resonant laser beam that initiates non-adiabatic coupling between the ground and first excited electronic potential energy surfaces of this ionic system. The underlying time-independent coupled-channels calculations allowed us to treat the non-adiabatic nuclear dynamics, dominated by two light-induced conical intersections, exactly. In particular, our state-of-the-art calculations showed the presence of interferences between pathways around two conical intersections. We have shown that these laser-induced conical intersections can significantly increase the atom-ion chemical reactivity at ultracold collision energies and relatively small intensities of the dressing laser. The expected rate coefficients should be easily detectable in current experimental setups. We also investigated charge exchange when the conical intersections were removed. The results of those studies showed that the conical intersections lead to noticeable differences in the reactive charge-exchange reaction.

Acknowledgements

Work at Temple University is supported by the U.S. Air Force Office of Scientific Research Grants No. FA9550-21-1-0153 and No. FA9550-19-1-0272 and the NSF Grant No. PHY-1908634.

[1] Born, M.; Oppenheimer, R. Zur Quantentheorie der Moleküle. *Ann. Phys.* **1927**, *84*, 457.

[2] Baer, M. *Beyond Born-Oppenheimer: Electronic Non-adiabatic Coupling Terms and Conical Intersections*; John Wiley & Sons, New York, 2006.

[3] Domcke, W.; Yarkony, D.; Köppel, H. *Conical Intersections: Electronic Structure, Dynamics & Spectroscopy*; Advanced Series in Physical Chemistry; World Scientific, Singapore, 2004; Vol. 15.

[4] Domcke, W.; Yarkony, D.; Köppel, H. *Conical Intersections: Theory, Computation and Experiment*; Advanced Series in Physical Chemistry; World Scientific Publishing Company, 2011; Vol. 17.

[5] Zhu, X.; Yarkony, D. R. Non-adiabaticity: the importance of conical intersections. *Mol. Phys.* **2016**, *114*, 1983–2013.

[6] Klessinger, M.; Michl, J. *Excited States and the Photochemistry of Organic Molecules*; VCH: New York, 1995.

[7] Peleg, O.; Bartal, G.; Freedman, B.; Manela, O.; Segev, M.; Christodoulides, D. N. Conical Diffraction and Gap Solitons in Honeycomb Photonic Lattices. *Phys. Rev. Lett.* **2007**, *98*, 103901.

[8] Leone, R.; Lévy, L. P.; Lafarge, P. Cooper-Pair Pump as a Quantized Current Source. *Phys. Rev. Lett.* **2008**, *100*, 117001.

[9] Moiseyev, N.; Šindelka, M.; Cederbaum, L. S. Laser-induced conical intersections in molecular optical lattices. *J. Phys. B* **2008**, *41*, 221001.

[10] Moiseyev, N.; Šindelka, M. The effect of polarization on the light-induced conical intersection phenomenon. *J.*

Phys. B **2011**, *44*, 111002.

[11] Šindelka, M.; Moiseyev, N.; Cederbaum, L. S. Strong impact of light-induced conical intersections on the spectrum of diatomic molecules. *J. Phys. B* **2011**, *44*, 045603.

[12] Szidarovszky, T.; Halász, G. J.; Császár, A. G.; Cederbaum, L. S.; Vibók, Á. Conical intersections induced by quantum light: Field-dressed spectra from the weak to the ultrastrong coupling regimes. *J. Phys. Chem. Lett.* **2018**, *9*, 6215–6223.

[13] Szidarovszky, T.; Halász, G. J.; Császár, A. G.; Cederbaum, L. S.; Vibók, Á. Direct signatures of light-induced conical intersections on the field-dressed spectrum of Na_2 . *J. Phys. Chem. Lett.* **2018**, *9*, 2739–2745.

[14] Demekhin, P. V.; Chiang, Y.; Cederbaum, L. S. Resonant Auger decay of core-excited C^*O molecules in intense x-ray laser fields. *Phys. Rev. A* **2011**, *84*, 033417.

[15] Demekhin, P. V.; Cederbaum, L. S. Resonant Auger decay of core-excited CO molecules in intense x-ray laser pulses: the $\text{O}(1s \rightarrow \pi^*)$ excitation. *J. Phys. B* **2013**, *46*, 164008.

[16] Wallis, A. O. G.; Hutson, J. M. Optically induced conical intersections in traps for ultracold atoms and molecules. *Phys. Rev. A* **2011**, *84*, 051402.

[17] Wüster, S.; Eisfeld, A.; Rost, J. M. Conical Intersections in an Ultracold Gas. *Phys. Rev. Lett.* **2011**, *106*, 153002.

[18] Tóth, A.; Csehi, A.; Halász, G. J.; Vibók, A. Photodissociation dynamics of the LiF molecule: Two- and three-state descriptions. *Phys. Rev. A* **2019**, *99*, 043424.

[19] Halász, G. J.; Vibók, A.; Moiseyev, N.; Cederbaum, L. S. Nuclear-wave-packet quantum interference in the intense laser dissociation of the D_2^+ molecule. *Phys. Rev. A* **2013**, *88*, 043413.

[20] Halász, G. J.; Vibók, Á.; Cederbaum, L. S. Direct signature of light-induced conical intersections in diatomics. *J. Phys. Chem. Lett.* **2015**, *6*, 348–354.

[21] Csehi, A.; Halász, G. J.; Cederbaum, L. S.; Vibók, A. Towards controlling the dissociation probability by light-induced conical intersections. *Faraday Discuss.* **2016**, *194*, 479–493.

[22] Csehi, A.; Halász, G. J.; Cederbaum, L. S.; Vibók, A. Competition between light-induced and intrinsic nonadiabatic phenomena in diatomics. *J. Phys. Chem. Lett.* **2019**, *7*, 1624–1630.

[23] Csehi, A.; Vendrell, O.; Halász, G. J.; Vibók, Á. Competition between collective and individual conical intersection dynamics in an optical cavity. *New J. Phys.* **2022**, *24*, 073022.

[24] Kim, J.; Tao, H.; White, J. L.; Petrovic, V. S.; Martinez, T. J.; Bucksbaum, P. H. Control of 1, 3-cyclohexadiene photoisomerization using light-induced conical intersections. *J. Phys. Chem. A* **2012**, *116*, 2758–2763.

[25] Corrales, M.; González-Vázquez, J.; Balerdi, G.; Solá, I. R.; De Nalda, R.; Bañares, L. Control of ultrafast molecular photodissociation by laser-field-induced potentials. *Nat. Chem.* **2014**, *6*, 785–790.

[26] Natan, A.; Ware, M. R.; Prabhudesai, V. S.; Lev, U.; Bruner, B. D.; Heber, O.; Bucksbaum, P. H. Observation of Quantum Interferences via Light-Induced Conical Intersections in Diatomic Molecules. *Phys. Rev. Lett.* **2016**, *116*, 143004.

[27] Kübel, M.; Spanner, M.; Dube, Z.; Naumov, A. Y.; Chelkowski, S.; Bandrauk, A. D.; Vrakking, M. J.; Corkum, P. B.; Villeneuve, D.; Staudte, A. Probing multiphoton light-induced molecular potentials. *Nat. Commun.* **2020**, *11*, 1–8.

[28] Thomas, R.; Roberts, K.; Tiesinga, E.; Wade, A.; Blakie, P.; Deb, A.; Kjærgaard, N. Multiple scattering dynamics of fermions at an isolated p-wave resonance. *Nat. Commun.* **2016**, *7*, 12069.

[29] Vitlina, R. Z.; Chaplik, A. V.; Entin, M. V. Nonresonant charge transfer in the field of an intense light wave. *Sov. Phys.-JETP* **1975**, *40*, 472–479.

[30] Copeland, D. A.; Tang, C. L. Photon-assisted nonresonant charge exchange: A simple molecular model. *J. Chem. Phys.* **1976**, *65*, 3161.

[31] Copeland, D. A.; Tang, C. L. On the optimal photon energy for photon-assisted nonresonant charge exchange. *J. Chem. Phys.* **1977**, *66*, 5126.

[32] George, T. F. Laser-Stimulated Molecular Dynamics and Rate Processes. *J. Phys. Chem.* **1982**, *86*, 10.

[33] T-S, H.; Laughlin, C. Laser-assisted charge-transfer reactions ($\text{Li}^{3+} + \text{H}$): Coupled dressed- quasimolecular-state approach. *Phys. Rev. A* **1985**, *45*, 122.

[34] Hsu, Y. P.; Kimura, M.; Olson, R. E. Laser-assisted charge-transfer collisions: $\text{K}^+ + \text{Na}$. *Phys. Rev. A* **1985**, *31*, 576.

[35] Sussman, B. J.; Townsend, D.; Ivanov, M. Y.; Stolow, A. Dynamic Stark Control of Photochemical Processes. *Science* **2006**, *314*, 278.

[36] Hall, F. H. J.; Aymar, M.; Bouloufa-Maafa, N.; Dulieu, O.; Willitsch, S. Light-Assisted Ion-Neutral Reactive Processes in the Cold Regime: Radiative Molecule Formation versus Charge Exchange. *Phys. Rev. Lett.* **2011**, *107*, 243202.

[37] Petrov, A.; Makrides, C.; Kotochigova, S. Laser controlled charge-transfer reaction at low temperatures. *J. Chem. Phys.* **2017**, *146*, 084304.

[38] Mills, M.; Puri, P.; Li, M.; Schowalter, S. J.; Dunning, A.; Schneider, C.; Kotochigova, S.; Hudson, E. R. Engineering Excited-State Interactions at Ultracold Temperatures. *Phys. Rev. Lett.* **2019**, *122*, 233401.

[39] Li, M.; Mills, M.; Puri, P.; Petrov, A.; Hudson, E. R.; Kotochigova, S. Excitation-assisted nonadiabatic charge-transfer reaction in a mixed atom-ion system. *Phys. Rev. A* **2019**, *99*, 062706.

[40] Li, H.; Jyothi, S.; Li, M.; Kłos, J.; Petrov, A.; Brown, K. R.; Kotochigova, S. Photon-mediated charge exchange reactions between ${}^{39}\text{K}$ atoms and ${}^{40}\text{Ca}^+$ ions in a hybrid trap. *Phys. Chem. Chem. Phys.* **2020**, *22*, 10870–10881.

[41] Yarkony, D. R. Conical Intersections: Diabolical and Often Misunderstood. *Acc. Chem. Res.* **1998**, *31*, 511–518.

[42] Kramida, A.; Ralchenko, Y.; Reader, J.; team, N. A. NIST Atomic Spectra Database (ver. 5.0). <http://physics.nist.gov/asd>, <http://physics.nist.gov/asd>.

[43] Zrafi, W.; Ladjimi, H.; Said, H.; Berriche, H.; Tomza, M. Ab initio electronic structure and prospects for the formation of ultracold calcium–alkali-metal-atom molecular ions. *New J. Phys.* **2020**, *22*, 073015.

[44] Cohen-Tannoudji, C.; Dupont-Roc, J.; Grynberg, G. *Atom-Photon Interactions: Basic Processes and Applications*; John Wiley & Sons, New York, 1992.

Supplemental Material: Quantum Control of Atom-Ion Charge Exchange via Light-induced Conical Intersections

Hui Li,^{1,*} Ming Li,¹ Alexander Petrov,¹ Eite Tiesinga,² and Svetlana Kotochigova^{1,†}

¹*Department of Physics, Temple University, Philadelphia, Pennsylvania 19122, USA*

²*Joint Quantum Institute, National Institute of Standards and Technology
and University of Maryland, Gaithersburg, Maryland 20899, USA*

A. The electronic structure of the KCa^+ molecule

In this paper we focus on two electronic potentials of the KCa^+ molecule, the ground state $\text{X}^1\Sigma^+$ potential and the excited $\text{A}^1\Sigma^+$ potential. We calculated these potentials using the non-relativistic multi-reference configuration interaction (MRCI) method as implemented in the MOLPRO program [?]. These calculations provide us with the electronic transition dipole moment between the two states as well. The inner-shell electrons for both K and Ca are described by the Stevens-Basch-Krauss-Jansien-Cundari (SBKJC) effective core potentials (ECP) [?], leaving only two valence electrons in the active space. The polarization of the effective cores is modeled via the core polarization potential (CPP) described in Ref. [?]. For the CPP, we use the static dipole polarizabilities of K^+ and Ca^{2+} , which are 5.472 a.u. [?] and 3.522 a.u. [?] respectively. Here, a.u. is an abbrevi-

ation for atomic unit. Müller/Meyer type cutoff functions are used with their exponents fitted to the asymptotic energies at large separation R , which yields the values 0.383 a.u. and 0.465 a.u. for K and Ca, respectively. For K we use the large 7s5p7d2f uncontracted Gaussian basis set from Ref. [?]. For Ca we use the contracted and optimized 9s7p6d/[7s6p6d] basis set from Ref. [?] augmented by three sets of f and one set of g polarization functions [?]. The contractions are specified in the square bracket. The multi-configurational self-consistent field (MCSCF) [? ?] method is used to obtain molecular orbitals, followed by a full configuration interaction calculation (MRCI) with two-electron excitations.

Figure 1(a) shows the MRCI potential energies for the $\text{X}^1\Sigma^+$ and $\text{A}^1\Sigma^+$ states as a function of interatomic separation. Figure 1(b) shows the electric transition dipole moment between these states. Data for this figure are found in Tables I, II, III, and IV.

* Present address: JILA, University of Colorado, Boulder, Col-

orado 80309, USA

† skotoch@temple.edu

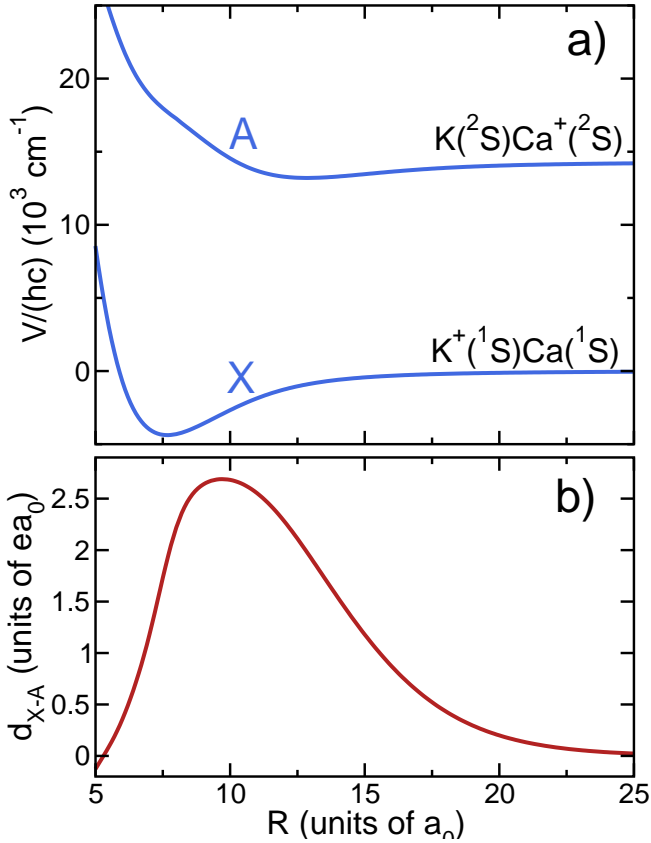


FIG. 1. (a) Non-relativistic $X^1\Sigma^+$ and $A^1\Sigma^+$ Born-Oppenheimer potentials of KCa^+ as functions of interatomic separation R . Asymptotic atomic configurations are given on the right hand side of the panel. The zero of energy is at the $\text{K}^+({}^1\text{S}) + \text{Ca}(4s^2 {}^1\text{S})$ dissociation limit. (b) R -dependent transition dipole moment between the $X^1\Sigma^+$ and $A^1\Sigma^+$ states.

TABLE I. Part I: The $X^1\Sigma^+$ and $A^1\Sigma^+$ potential energy curves of KCa^+ .

R/a_0	V_X/hc	V_A/hc									
	(cm $^{-1}$)	(cm $^{-1}$)		(cm $^{-1}$)	(cm $^{-1}$)		(cm $^{-1}$)	(cm $^{-1}$)		(cm $^{-1}$)	(cm $^{-1}$)
4.0	21446.976	35486.971	11.0	-1863.422	13696.072	17.6	-209.574	13851.081	24.2	-54.460	14191.014
4.1	20488.572	34659.956	11.1	-1793.755	13636.918	17.7	-204.428	13862.210	24.3	-53.539	14192.888
4.2	19379.026	33838.999	11.2	-1726.303	13582.236	17.8	-199.447	13873.048	24.4	-52.637	14194.719
4.3	18146.077	33032.147	11.3	-1661.070	13531.919	17.9	-194.623	13883.598	24.5	-51.755	14196.508
4.4	16820.757	32243.531	11.4	-1598.049	13485.849	18.0	-189.951	13893.866	24.6	-50.891	14198.256
4.5	15434.699	31474.418	11.5	-1537.225	13443.898	18.1	-185.423	13903.856	24.7	-50.046	14199.965
4.6	14017.881	30724.355	11.6	-1478.577	13405.928	18.2	-181.036	13913.573	24.8	-49.218	14201.635
4.7	12597.047	29992.166	11.7	-1422.076	13371.799	18.3	-176.782	13923.024	24.9	-48.407	14203.268
4.8	11194.851	29276.652	11.8	-1367.690	13341.361	18.4	-172.658	13932.212	25.0	-47.613	14204.865
4.9	9829.609	28577.007	11.9	-1315.378	13314.465	18.5	-168.658	13941.145	25.1	-46.835	14206.427
5.0	8515.474	27892.992	12.0	-1265.098	13290.954	18.6	-164.777	13949.828	25.2	-46.073	14207.954
5.1	7262.860	27224.956	12.1	-1216.801	13270.673	18.7	-161.012	13958.266	25.3	-45.327	14209.448
5.2	6078.972	26573.759	12.2	-1170.438	13253.463	18.8	-157.357	13966.466	25.4	-44.596	14210.909
5.3	4968.351	25940.656	12.3	-1125.955	13239.167	18.9	-153.809	13974.434	25.5	-43.879	14212.339
5.4	3933.382	25327.141	12.4	-1083.297	13227.629	19.0	-150.364	13982.176	25.6	-43.177	14213.738
5.5	2974.744	24734.819	12.5	-1042.407	13218.694	19.1	-147.018	13989.697	25.7	-42.489	14215.107
5.6	2091.785	24165.268	12.6	-1003.226	13212.208	19.2	-143.768	13997.004	25.8	-41.815	14216.446
5.7	1282.834	23619.935	12.7	-965.697	13208.022	19.3	-140.609	14004.103	25.9	-41.154	14217.758
5.8	545.460	23100.053	12.8	-929.759	13205.987	19.4	-137.540	14010.999	26.0	-40.507	14219.042
5.9	-123.325	22606.577	12.9	-895.353	13205.962	19.5	-134.556	14017.697	26.1	-39.872	14220.299
6.0	-726.889	22140.151	13.0	-862.421	13207.805	19.6	-131.656	14024.205	26.2	-39.249	14221.529
6.1	-1268.846	21701.095	13.1	-830.904	13211.383	19.7	-128.835	14030.527	26.3	-38.639	14222.734
6.2	-1752.937	21289.407	13.2	-800.744	13216.563	19.8	-126.091	14036.668	26.4	-38.041	14223.914
6.3	-2182.947	20904.775	13.3	-771.887	13223.221	19.9	-123.422	14042.635	26.5	-37.454	14225.070
6.4	-2562.629	20546.606	13.4	-744.275	13231.235	20.0	-120.825	14048.432	26.6	-36.878	14226.203
6.5	-2895.660	20214.046	13.5	-717.856	13240.489	20.1	-118.298	14054.065	26.7	-36.314	14227.312
6.6	-3185.592	19906.013	13.6	-692.577	13250.870	20.2	-115.838	14059.538	26.8	-35.760	14228.398
6.7	-3435.836	19621.221	13.7	-668.387	13262.274	20.3	-113.444	14064.857	26.9	-35.217	14229.463
6.8	-3649.637	19358.205	13.8	-645.238	13274.598	20.4	-111.112	14070.026	27.0	-34.685	14230.507
6.9	-3830.063	19115.346	13.9	-623.082	13287.747	20.5	-108.841	14075.050	27.1	-34.162	14231.529
7.0	-3980.003	18890.891	14.0	-601.873	13301.629	20.6	-106.630	14079.933	27.2	-33.649	14232.532
7.1	-4102.162	18682.981	14.1	-581.567	13316.158	20.7	-104.475	14084.680	27.3	-33.146	14233.514
7.2	-4199.062	18489.672	14.2	-562.123	13331.252	20.8	-102.376	14089.296	27.4	-32.652	14234.477
7.3	-4273.048	18308.971	14.3	-543.500	13346.835	20.9	-100.330	14093.783	27.5	-32.168	14235.421
7.4	-4326.294	18138.879	14.4	-525.659	13362.833	21.0	-98.336	14098.147	27.6	-31.692	14236.347
7.5	-4360.809	17977.438	14.5	-508.563	13379.180	21.1	-96.392	14102.391	27.7	-31.225	14237.255
7.6	-4378.445	17822.790	14.6	-492.178	13395.811	21.2	-94.497	14106.519	27.8	-30.767	14238.145
7.7	-4380.911	17673.232	14.7	-476.468	13412.669	21.3	-92.649	14110.535	27.9	-30.317	14239.019
7.8	-4369.776	17527.262	14.8	-461.403	13429.697	21.4	-90.847	14114.442	28.0	-29.875	14239.875
8.0	-4312.363	17261.643	14.9	-446.951	13446.845	21.5	-89.090	14118.244	28.1	-29.442	14240.715
8.2	-4216.410	16957.669	15.0	-433.083	13464.066	21.6	-87.375	14121.944	28.2	-29.016	14241.539
8.3	-4156.726	16815.563	15.1	-419.772	13481.315	21.7	-85.702	14125.545	28.3	-28.598	14242.348
8.4	-4090.524	16673.014	15.2	-406.991	13498.552	21.8	-84.070	14129.050	28.4	-28.188	14243.141

TABLE II. Part II: The $X^1\Sigma^+$ and $A^1\Sigma^+$ potential energy curves of KCa^+ .

R/a_0	V_X/hc	V_A/hc									
	(cm $^{-1}$)	(cm $^{-1}$)		(cm $^{-1}$)	(cm $^{-1}$)		(cm $^{-1}$)	(cm $^{-1}$)		(cm $^{-1}$)	(cm $^{-1}$)
8.5	-4018.671	16530.043	15.3	-394.715	13515.742	21.9	-82.477	14132.463	28.5	-27.784	14243.920
8.6	-3941.963	16386.798	15.4	-382.921	13532.849	22.0	-80.922	14135.786	28.6	-27.388	14244.684
8.7	-3861.128	16243.526	15.5	-371.586	13549.844	22.1	-79.404	14139.023	28.7	-27.000	14245.433
8.8	-3776.837	16100.545	15.6	-360.687	13566.699	22.2	-77.922	14142.175	28.8	-26.618	14246.169
8.9	-3689.701	15958.224	15.7	-350.206	13583.388	22.3	-76.475	14145.245	28.9	-26.242	14246.892
9.0	-3600.282	15816.961	15.8	-340.122	13599.890	22.4	-75.062	14148.237	29.0	-25.874	14247.601
9.1	-3509.091	15677.167	15.9	-330.417	13616.184	22.5	-73.681	14151.152	29.1	-25.511	14248.297
9.2	-3416.598	15539.253	16.0	-321.074	13632.253	22.6	-72.333	14153.993	29.2	-25.155	14248.980
9.3	-3323.228	15403.620	16.1	-312.077	13648.080	22.7	-71.016	14156.762	29.3	-24.806	14249.651
9.5	-3135.373	15140.684	16.2	-303.409	13663.653	22.8	-69.729	14159.462	29.4	-24.462	14250.310
9.6	-3041.559	15014.060	16.3	-295.056	13678.959	22.9	-68.471	14162.094	29.5	-24.124	14250.958
9.7	-2948.214	14891.067	16.4	-287.003	13693.990	23.0	-67.242	14164.660	29.6	-23.793	14251.593
9.9	-2763.940	14656.966	16.5	-279.238	13708.735	23.1	-66.041	14167.163	29.7	-23.466	14252.217
10.0	-2673.450	14546.273	16.6	-271.747	13723.190	23.2	-64.867	14169.606	29.8	-23.146	14252.831
10.1	-2584.311	14440.039	16.7	-264.519	13737.347	23.3	-63.719	14171.988	29.9	-22.831	14253.433
10.2	-2496.684	14338.388	16.8	-257.543	13751.204	23.4	-62.597	14174.312	30.0	-22.521	14254.025
10.3	-2410.710	14241.415	16.9	-250.806	13764.757	23.5	-61.499	14176.580	32.5	-16.235	14265.948
10.4	-2326.513	14149.188	17.0	-244.299	13778.004	23.6	-60.426	14178.793	35.0	-11.993	14273.903
10.5	-2244.197	14061.746	17.1	-238.013	13790.946	23.7	-59.376	14180.953	37.5	-9.045	14279.389
10.6	-2163.851	13979.103	17.2	-231.937	13803.580	23.8	-58.349	14183.062	40.0	-6.943	14283.276
10.7	-2085.548	13901.253	17.3	-226.064	13815.909	23.9	-57.345	14185.121	45.0	-4.275	14288.183
10.8	-2009.347	13828.166	17.4	-220.384	13827.933	24.0	-56.362	14187.132	50.0	-2.758	14290.958
10.9	-1935.294	13759.794	17.5	-214.890	13839.657	24.1	-55.401	14189.096			

TABLE III. Part I: Electric transition dipole moment between the $X^1\Sigma^+$ and $A^1\Sigma^+$ states of KCa^+ .

R/a_0	$d/(ea_0)$	R/a_0	$d/(ea_0)$	R/a_0	$d/(ea_0)$	R/a_0	$d/(ea_0)$
8.0	2.219570	14.0	1.540030	19.6	0.234320	25.2	0.021189
8.1	2.293330	14.1	1.502300	19.7	0.225129	25.3	0.020253
8.2	2.358300	14.2	1.464860	19.8	0.216268	25.4	0.019357
8.4	2.463930	14.3	1.427760	19.9	0.207726	25.5	0.018500
8.6	2.541950	14.4	1.391030	20.0	0.199494	25.6	0.017679
8.7	2.572480	14.5	1.354690	20.1	0.191563	25.7	0.016894
8.8	2.598270	14.6	1.318770	20.2	0.183921	25.8	0.016143
8.9	2.619900	14.7	1.283300	20.3	0.176563	25.9	0.015424
9.0	2.637890	14.8	1.248290	20.4	0.169477	26.0	0.014736
9.1	2.652670	14.9	1.213780	20.5	0.162656	26.1	0.014078
9.2	2.664580	15.0	1.179790	20.6	0.156091	26.2	0.013449
9.3	2.673930	15.1	1.146320	20.7	0.149772	26.3	0.012847
9.5	2.685810	15.2	1.113400	20.8	0.143692	26.4	0.012271
9.6	2.688690	15.3	1.081030	20.9	0.137844	26.5	0.011721
9.7	2.689680	15.4	1.049240	21.0	0.132218	26.6	0.011194
9.9	2.686360	15.5	1.018030	21.1	0.126808	26.7	0.010690
10.0	2.682160	15.6	0.987412	21.2	0.121607	26.8	0.010208
10.1	2.676320	15.7	0.957396	21.3	0.116606	26.9	0.009748
10.2	2.668860	15.8	0.927988	21.4	0.111799	27.0	0.009307
10.3	2.659810	15.9	0.899192	21.5	0.107179	27.1	0.008866
10.4	2.649170	16.0	0.871014	21.6	0.102741	27.2	0.008484
10.5	2.636980	16.1	0.843456	21.7	0.098476	27.3	0.008099
10.6	2.623240	16.2	0.816520	21.8	0.094378	27.4	0.007732
10.7	2.607960	16.3	0.790206	21.9	0.090443	27.5	0.007380
10.8	2.591170	16.4	0.764515	22.0	0.086664	27.6	0.007045
10.9	2.572890	16.5	0.739446	22.1	0.083034	27.7	0.006723
11.0	2.553140	16.6	0.714995	22.2	0.079550	27.8	0.006417
11.1	2.531960	16.7	0.691161	22.3	0.076204	27.9	0.006124
11.2	2.509370	16.8	0.667939	22.4	0.072993	28.0	0.005844
11.3	2.485420	16.9	0.645324	22.5	0.069912	28.1	0.005576
11.4	2.460150	17.0	0.623313	22.6	0.066954	28.2	0.005320
11.5	2.433610	17.1	0.601900	22.7	0.064116	28.3	0.005076
11.6	2.405850	17.2	0.581070	22.8	0.061394	28.4	0.004843
11.7	2.376930	17.3	0.560829	22.9	0.058782	28.5	0.004620
11.8	2.346900	17.4	0.541157	23.0	0.056277	28.6	0.004407
11.9	2.315830	17.5	0.522055	23.1	0.053874	28.7	0.004204
12.0	2.283790	17.6	0.503510	23.2	0.051569	28.8	0.004010
12.1	2.250830	17.7	0.485514	23.3	0.049361	28.9	0.003824
12.2	2.217030	17.8	0.468058	23.4	0.047242	29.0	0.003647
12.3	2.182450	17.9	0.451132	23.5	0.045212	29.1	0.003478
12.4	2.147170	18.0	0.434726	23.6	0.043265	29.2	0.003317
12.5	2.111250	18.1	0.418830	23.7	0.041399	29.3	0.003162
12.6	2.074770	18.2	0.403434	23.8	0.039610	29.4	0.003015
12.7	2.037790	18.3	0.388526	23.9	0.037896	29.5	0.002875
12.8	2.000380	18.4	0.374097	24.0	0.036254	29.6	0.002741
12.9	1.962610	18.5	0.360135	24.1	0.034680	29.7	0.002613
13.0	1.924540	18.6	0.346630	24.2	0.033172	29.8	0.002490

TABLE IV. Part II: Electric transition dipole moment between the $X^1\Sigma^+$ and $A^1\Sigma^+$ states of KCa^+ .

R/a_0	$d/(ea_0)$	R/a_0	$d/(ea_0)$	R/a_0	$d/(ea_0)$	R/a_0	$d/(ea_0)$
13.1	1.886230	18.7	0.333571	24.3	0.031727	29.9	0.002374
13.2	1.847740	18.8	0.320947	24.4	0.030344	30.0	0.002262
13.3	1.809140	18.9	0.308747	24.5	0.029018	32.5	0.000668
13.4	1.770470	19.0	0.296960	24.6	0.027749	35.0	0.000190
13.5	1.731800	19.1	0.285576	24.7	0.026534	37.5	0.000054
13.6	1.693170	19.2	0.274584	24.8	0.025370	40.0	0.000017
13.7	1.654630	19.3	0.263972	24.9	0.024255	45.0	0.000005
13.8	1.616230	19.4	0.253732	25.0	0.023188	50.0	0.000005
13.9	1.578020	19.5	0.243851	25.1	0.022167		